(NASA-TM-102265) IN-FLIGHT MEASUREMENT OF PROPELLER NOISE ON THE FUSELAGE OF AN AIRPLANE (NASA. Lewis Research Center) 58 p
CSCL 20A
N89-25875
Unclas
G3/71 0219563

In-Flight Measurement of Propeller Noise on the Fuselage of an Airplane

Frederic G. Pla
Sverdrup Technology, Inc.
NASA Lewis Research Center Group
Cleveland, Ohio 44135

and

Richard Ranaudo and Richard P. Woodward
National Aeronautics and Space Administration
Lewis Research Center
Cleveland, Ohio 44135

ABSTRACT

In-flight measurements of propeller noise on the fuselage of an OV-10A airplane were obtained using a horizontal and a vertical microphone array. A wide range of flight conditions were tested including changes in angle of attack, sideslip angle, power coefficient, helical tip Mach number and advance ratio, and propeller direction of rotation. Results show a dependence of the level and directivity of the tones on the angle of attack and on the sideslip angle with the propeller direction of rotation, which is similar to results obtained in wind tunnel tests with advanced propeller designs. The level of the tones at each microphone increases with increasing angle of attack for inboard-down propeller rotation and decreases for inboard-up rotation. The level also increases with increasing sideslip angle for both propeller directions of rotation. Increasing the power coefficient results in a slight increase in the level of the tones. A strong shock wave is generated by the propeller blade even at relatively low helical tip Mach numbers resulting in high harmonic levels. As the helical tip Mach number and the advance ratio are increased, the level of the higher harmonics increases much faster than the level of the blade passage frequency.

LIST OF SYMBOLS

C_p Power Coefficient ($\frac{P}{\rho n^3 D^5}$)

c Speed of sound

D Propeller diameter

J Advance Ratio ($\frac{U_T}{nD}$)

M_a Axial Mach number ($\frac{U_T}{c}$)

M_h Helical tip Mach number ($\frac{\sqrt{U_T^2 + U_P^2}}{c}$)

n Propeller revolutions per second

P Total Power

r Propeller blade radial coordinate

U_P Propeller rotational speed ($n\pi D$)

U_T Airplane true air speed

$\vec{V}$ Inflow velocity vector

V_n Inflow velocity in the propeller plane normal to the blade radius

v_1 Component of $\vec{V}$ parallel to the left propeller axis

v_2 Horizontal component of $\vec{V}$ in the left propeller plane

v_3 Vertical component of $\vec{V}$ in the left propeller plane

x Horizontal coordinate along the left propeller axis (positive upstream)

y Horizontal coordinate in the left propeller plane (positive away from the airplane fuselage)

z Vertical coordinate in the left propeller plane (positive upward)

α_{av}	Angle of attack at each rake station averaged over neighboring test points with similar α_{prop}
α_b	Propeller blade angle of attack
α_{boom}	Airplane angle of attack measured at the nose boom
α_p	Local angle of attack at the propeller plane (pitch angle) between the propeller axis and the incoming flow.
α_{prop}	Inflow angle of attack at the propeller plane averaged over all rake stations
α_{var}	Term proportional to the magnitude of the variation in α_{av} between the top and the bottom of the propeller plane
β	Airplane sideslip angle measured at the nose boom
β_b	Propeller blade pitch angle
β_p	Sideslip angle at the propeller plane (yaw angle) between the propeller axis and the incoming flow
$\Delta\alpha$	Circumferential variation of the angle of attack at the propeller plane
ρ	Local air density
φ	Angle between the local velocity vector and the propeller plane
ψ	Propeller azimuthal angle
ω	Propeller blade angular velocity

1. Introduction

In recent years, much work has been done on propeller noise due to the interest in advanced propeller concepts. High-speed propeller aircraft are expected to fly at speeds comparable to present modern subsonic commercial transports, and at a 50% to 60% savings in fuel relative to current technology engines [1].

However, the noise of such aircraft is a strong concern both inside and outside the cabin. The take-off and landing noise is especially critical to communities around airports and has been studied extensively in recent papers (see Refs. [2] to [4]).

Because of the non-zero engine axis angle of attack at take-off and landing, the noise generated by a propeller differs at take-off and landing conditions from that at cruise condition. This results in a non-constant blade angle of attack as the propeller goes through a 360 degree rotation. As a result, the directivity of the propeller is not symmetrical with respect to the propeller axis (see Refs. [2] to [5]).

Variations in the blade advance ratio, helical tip Mach number, and blade loading also affect the overall noise generated.

Finally, the propeller direction of rotation has some effect on the noise level inside the cabin. Most of the noise generated by a propeller blade radiates in a direction normal to the blade radius and in the direction of blade travel. Therefore, as a result of the aircraft angle of attack and wing upwash, the blade coming towards the fuselage has a higher loading in the case of inboard-down propeller rotation and is therefore noisier than in the case of inboard-up rotation

(see Refs. [4] and [5]). Also, cabin noise levels are usually lower in the case of a propeller rotating inboard-up due to the floor structure helping to block the sound transmitted to the cabin [6].

This report presents results from in-flight tests of an OV–10A Bronco aircraft to study the influence of airplane pitch and yaw angle, blade advance ratio, helical tip Mach number, loading, and direction of rotation on the noise levels measured on the aircraft fuselage.

2. Test Configuration

This section describes the aircraft and the instrumentation used in this study as well as the test procedures and the data acquisition and reduction system.

2.1. Test Aircraft

The test aircraft chosen for this study was an OV–10A Bronco (see Figure 1). The OV–10A, designed for tactical air support, is powered by two Garrett-Air Research T–76–G series single–shaft turboprop engines rated at 715-shaft-horsepower each. The Hamilton Standard 1027A–0 aluminum propellers are 3-blade, 2.59-meters diameter, full-reversible, full-feathering, and constant speed. The clearance between propeller tips and fuselage is 0.46 meter. In order to minimize engine propeller torque effects, the gear boxes are such that the propellers are counterrotating, the left propeller rotating clockwise, and the right propeller rotating counter-clockwise as viewed from a downstream position (i.e., both propellers rotating inboard-down). This last feature was a determining factor in selecting the OV–10A as a test platform in that the engine sets can be readily interchanged to change propeller direction of rotation. Moreover, the high

maneuverability of the OV–10A is particularly suited to achieve a wide range of flight parameters with resulting range of propeller noise generation mechanisms.

2.2. Aircraft Acoustic Instrumentation

A horizontal and a vertical microphone array were installed on the left side of the airplane fuselage as shown in Figure 2.

The microphones positions with respect to the propeller axis and plane of rotation are given in Table I.

The x, y, z orthogonal coordinate system has its origin at the center of the left propeller disk and is aligned with the propeller axis and plane of rotation as shown in Figure 3. x is the horizontal coordinate along the propeller axis (positive upstream), y is the horizontal coordinate in the propeller plane (positive away from the fuselage), and z is the vertical coordinate in the propeller plane (positive upward). The corresponding cylindrical coordinate system r, θ, ϕ is also shown in Figure 3.

Microphone positions for the horizontal array were chosen so that the microphones are parallel to the propeller axis and approximately 10 degrees apart from each other. For the vertical array, the microphones are also approximately 10 degrees apart and in the propeller plane. The actual microphones locations were selected with consideration of structural members on the aircraft.

An instrumentation rack consisting of signal conditioners, amplifiers, and a 14-channel FM tape recorder was mounted in the OV–10A cargo bay. For each test point, the automated data acquisition process was initiated by the pilot through the flip of a switch on the control panel. The signal going in and coming

out of the tape recorder was monitored by the flight test engineer in the back seat of the airplane.

2.3. Acoustic Data Reduction and Analysis

Averaged spectra were obtained for each microphone by playing the tape recorder through a 16-channel FFT-analyzer. The spectra were transferred to a computer where the amplitude and frequency of the first six multiples of the Blade Passage Frequency (BPF) were calculated. The rest of the analysis including calibration and plotting of the data was carried out using a spreadsheet-based program.

2.4. Aircraft Flight Instrumentation

The raw aerodynamic data used to calculate the flight parameters were measured using a flight test nose boom instrumented to measure aircraft angle of attack (pitch angle), aircraft sideslip angle (yaw angle), altitude, temperature, and air speed. The data were displayed on the pilot instrument panel and recorded using a cockpit-mounted motion picture camera synchronized with the acoustic data acquisition system.

2.5. Flight Data Calculation

The flight parameters of interest are the helical tip Mach number, the axial Mach number, the advance ratio, the power coefficient, the angle of attack, and the sideslip angle.

For the results shown in the next sections, the advance ratio, and the power coefficient were calculated using readings from the motion picture camera.

In order to minimise variations in the flight parameters J and C_p, the flight altitude, the indicated air speed, and the engine torque and RPM were calculated just before each flight using altitude weather data for the test area. This procedure allowed flight conditions for each test point to be replicated accurately so as to obtain good data repeatability from one day to the other. In some cases, flight parameters could not be kept constant during a test point such as in high speed dives. Such variations are indicated in this report when they occurred.

Due to a difference between the propeller axis (thrust line) and the aircraft fuselage reference line, two degrees were added to the airplane boom angle of attack measurements to obtain the propeller angle of attack (see Figure 4).

3. Propeller Blade Angle of Attack

This section describes the semi-empirical formulas used to calculate the blade angle of attack variation α_b as a function of the propeller azimuthal position ψ and the measured flight parameters.

The circumferentially varying propeller blade angle of attack α_b which depends on the airplane angle of attack α_{boom} and on distortions in the flow field around the aircraft such as the wing upwash is a major parameter in this study. Variations in α_b affect the cyclic loading of the blade which in turn affects the magnitude and the directivity of the noise generated.

The approach in this section can be summarised as follows:

First, a theoretical relationship is defined between the blade angle of attack α_b, and the local angle of attack α_p and sideslip angle β_p between the propeller axis and the incoming flow.

Next, empirical formulas are derived which relate α_p as a function of propeller azimuthal position ψ to the airplane angle of attack α_{boom} measured at the nose boom.

The final result is a series of semi-empirical formulas based on rake measurements which relate α_b to measured flight parameters. All the results presented here are for the 3/4 tip radius of the propeller.

3.1. Propeller Blade Angle of Attack Versus Flight Parameters, Including Local Pitch and Yaw Angles

As shown in Figure 5, the propeller blade angle of attack, α_b, relative to the inflow can be expressed as:

$$\alpha_b = \beta_b - \varphi \tag{1}$$

β_b is the 3/4 tip radius blade pitch angle and φ is the angle between the local velocity vector and the propeller plane.

For each flight condition, β_b was measured using pictures of the propeller taken with a high speed motion picture camera mounted on the back seat of the airplane.

φ is given by:

$$\varphi = \tan^{-1}\left(\frac{v_1}{V_a}\right) \tag{2}$$

v_1 is the component of the inflow velocity vector $\vec{V}$ parallel to the propeller axis and V_a is the inflow velocity in the propeller plane normal to the blade pitch change axis. From Figure 5, V_a can be expressed as:

$$V_a = r\omega + v_2 \sin(\psi) - v_3 \cos(\psi) \tag{3}$$

where r is the blade radial location (3/4 tip radius), ω is the blade angular velocity, and ψ is the blade azimuthal angle. v_2 and v_3 are the components of $\vec{V}$ in the propeller plane.

For a non-distorted inflow, the components v_1, v_2, and v_3 of $\vec{V}$ can be rewritten as:

$$\begin{aligned} v_1 &= |V| \cos(\beta_p) \cos(\alpha_p) \\ v_2 &= |V| \sin(\beta_p) \cos(\alpha_p) \\ v_3 &= |V| \sin(\alpha_p) \end{aligned} \tag{4}$$

α_p is the pitch angle or local angle of attack between the propeller axis and the incoming flow. β_p is the yaw or sideslip angle between the propeller axis and the incoming flow. α_p is positive when the airplane nose rotates upwards, and β_p is positive when the airplane is yawed to the left. The assumption is made that the magnitude $|V|$ of the inflow velocity vector $\vec{V}$ at the propeller blade is the same as the magnitude of the velocity vector obtained from measurements taken at the nose boom.

3.2. Angle of Attack at the Propeller Plane Versus Measured Airplane Angle of Attack

In this section, empirical formulas based on flow angle measurements with a wing-mounted rake are derived which relate α_p as a function of propeller azimuthal position ψ to the airplane angle of attack measured at the nose boom (α_{boom}). The result can then be used in Equations (1) to (4) to calculate the blade angle of attack α_b.

The local angle of attack α_p between the propeller axis and the incoming flow at the 3/4 tip radius of the propeller can be expressed as the sum of a constant term and a circumferentially varying term:

$$\alpha_p = \alpha_{prop} + \Delta\alpha \tag{5}$$

α_{prop} is the angle of attack averaged over the propeller plane and $\Delta\alpha$ is the circumferential variation of the angle of attack at the propeller plane.

As described in the following two sections, α_{prop} and $\Delta\alpha$ were evaluated experimentally. Raw inflow angle data were obtained using a tufted rake attached to the airplane wing. These data were used to derive an empirical relationship between α_{prop} and α_{boom}, and between $\Delta\alpha$ and α_{boom} as a function of the propeller azimuthal position ψ. Note that the flow angles measured with the rake are assumed constant with wing spanwise position.

3.2.1. Experimental Setup

Flights were made with the OV-10A equipped with a wing-mounted tufted rake as shown in Figure 4.

The 1.83-meters long rake was mounted vertically outboard of the right propeller and perpendicular to the aircraft fuselage reference line so that there was a 2-degree difference between the rake and the propeller plane. The center of the rake was in the propeller plane, 0.57 meter ahead of the leading edge of the wing. The angles between the tufts of yarn and the horizontal reference stripes were measured at seven different rake stations using photographs from a camera mounted on the back seat of the airplane. The position of the seven stations

used to average the inflow angle data are indicated by black dots on the rake in Figure 4 and are given in Table III.

Over 50 test points were taken for the angle of attack measured at the aircraft nose boom (α_{boom}) varying from −3 degrees to +16 degrees, and for an indicated air speed varying from 43 m/s to 129 m/s.

3.2.2. Relationship Between the Angle of Attack at the Propeller Plane and the Airplane Angle of Attack Measured at the Nose Boom

The expression for α_p is given in Equation (5) as the sum of the average angle of attack at the propeller plane α_{prop} and the circumferential variation of the angle of attack at the propeller plane $\Delta\alpha$.

The angle of attack at the propeller plane α_{prop} averaged over the seven rake stations is shown in Figure 6 for a range of α_{boom} similar to the range used during the acoustic testing. There is some scatter in the data primarily due to "random" variations of the inflow angle at some of the rake stations caused by local turbulence in the flow.

The quadratic fit of α_{prop} versus α_{boom} shown in Figure 6 is given by:

$$\alpha_{prop} = 0.037\,\alpha_{boom}^{\,2} + 0.928\,\alpha_{boom} + 2.415 \qquad (6)$$

Changes in air speed do not seem to have any significant effect on the relationship between α_{prop} and α_{boom}. This result is consistent with data from a simple two-dimensional potential flow analysis of the flow around the OV-10A wing.

$\Delta\alpha$ is the circumferential variation of the angle of attack at the propeller plane and takes into account the non-constant angle of attack at the propeller plane due to flow field distortions as illustrated by Figure 7.

Each curve in Figure 7 shows the angle of attack α_{av} at the propeller plane and at each rake station obtained by averaging nine neighboring data points (except for the curve with the highest angle of attack which was obtained by averaging seven points). As mentioned previously, averaging over several measurements was required to reduce the influence of "bad angle readings" at some of the rake stations.

For every curve in Figure 7, α_{av} is larger at the top than at the bottom of the propeller plane due to the wing upwash. An empirical formula for the angle of attack variation $\Delta\alpha$ as a function of the azimuthal position ψ was obtained using the 27 rake data points which correspond to the range of angles of attack for which acoustic tests were run (-3.5 degrees to 4.5 degrees):

$$\Delta\alpha = \alpha_{var}\left[0.678\sin^2(\psi) + 0.602\sin(\psi) - 0.180\right] \tag{7}$$

The term on the right-hand side inside the brackets is a quadratic fit of the angle of attack variation as a function of the azimuthal position.

α_{var} accounts for the increase in the magnitude of the variation in α_{av} between the top and the bottom of the propeller plane with increasing airplane angle of attack α_{boom} (see Figure 7). α_{var} is given by:

$$\alpha_{var} = 0.405\,\alpha_{prop} + 3.164 \tag{8}$$

3.3. Propeller Blade Angle of Attack Variation For a Typical Case

For each test point, the blade angle of attack α_b is given by Equations (1) to (4). Measured data are used for the sideslip angle β_p, the airplane speed V, the blade angular velocity ω, and the blade pitch angle β_b. Equations (5)

to (7) are used to calculate the local angle of attack at the propeller plane α_p as a function of the airplane angle of attack α_{boom} and the propeller asimuthal position ψ.

A plot of α_b versus ψ is shown in Figure 8 for a positive angle of attack ($\alpha_{prop} = 8.6$ degrees) with and without the effect of the wing upwash. The plot is for the left propeller rotating inboard-down, and for flight conditions typical of a low-speed, high angle of attack test.

The solid curve does not take the wing upwash into account. It was obtained by setting the circumferential variation of the angle of attack at the propeller plane $\Delta\alpha$ in Equation (5) to zero ($\alpha_p = \alpha_{prop}$). The dashed curve takes the wing upwash into account and was obtained by using Equations (5) to (8) to calculate α_p.

When α_p is constant and for inboard-down propeller direction of rotation, the variation in α_b is sinusoidal with a maximum at $\psi = 180$ degrees or when the blade is closest to the fuselage. When the wing upwash is included in the calculations (circumferentially varying α_p), the variation in α_b is not sinusoidal and the maximum occurs for $90 < \psi < 180$ when the blade is between the top vertical position and the horizontal position closest to the fuselage.

Because of safety considerations, an experimental rake study could not be carried out to look at the variation of the sideslip angle β_p at the propeller plane. Due to the close proximity between propeller and fuselage, and the large fuselage area, there is a blockage of the cross-flow. Thus, β_p is different from the angle measured at the airplane nose boom β. However, both angle variations

follow similar trends and good qualitative agreement is obtained between noise variation and sideslip angle variation as shown in a later section.

4. Acoustic Results

In this section, results are presented showing the influence of the angle of attack α_{boom}, the sideslip angle β, the power coefficient C_p, the advance ratio J and helical tip Mach number M_h, and the propeller direction of rotation on the noise generated on the OV–10A fuselage.

The test matrix shown in Table III takes advantage of the whole OV–10A flight envelope and was repeated for each propeller direction of rotation. Very good repeatability was obtained in the acoustic data from one flight to another.

4.1. General Considerations

The acoustic signatures and spectra recorded at two microphone positions are shown for two helical tip Mach numbers in Figures 9 and 10.

Results in Figure 9 are for a moderate helical tip Mach number M_h of 0.86, an axial Mach number M_a of 0.25, and inboard-up propeller direction rotation.

The waveform recorded ahead of the propeller by microphone #2 is fairly smooth and nearly all of the acoustic energy is at the Blade Passage Frequency (BPF) and the next two harmonics as shown in the spectrum below the waveform. The Overall Sound Pressure Level (OASPL) is 124 dB.

Microphone #6 is in the propeller plane and shows a much higher OASPL. A weak shock wave which translates into high harmonic levels is clearly visible on the plot of the time history. The OASPL is 135 dB. The presence of a shock on

the propeller blade for a relatively moderate helical tip Mach number is typical of the conventional straight thick blade used in general aviation aircraft.

The graph at the bottom of Figure 9 summarizes the results for all microphones. The Sound Pressure Levels (SPL) at the BPF and at the next five multiples of the BPF are plotted versus position in both horizontal and vertical arrays. The level of the tones was obtained from the harmonic peaks in the spectra and was corrected for windowing effects. The acoustic level is maximum slightly ahead of the propeller plane and decreases rapidly fore and aft of the propeller except for the BPF aft of the propeller plane. One possible explanation for the constant level of the BPF aft of the propeller is the presence of standing waves between the fuselage and the engine compartment which are parallel and about 1.4 meters away from each other as show in Figures 1 and 2. Away from the propeller plane, the BPF is the strongest contributor to the OASPL. In the propeller plane, all the tones are within 10 dB of each other.

Figure 10 shows results for a high M_h of 1.02 and an axial Mach number M_a of 0.60, well above the propeller design point. The waveforms recorded by both microphones have a much higher amplitude and a richer harmonic content than in the previous case (moderate M_h). The tone from the right engine propeller on the opposite side of the microphone array is clearly visible in the spectra from microphone #2. For each test point, the right engine RPM was kept at least 5% lower than the left engine RPM so that contributions from both propellers could be easily identified.

The waveform recorded by microphone #2 has a slightly higher harmonic content than the waveform shown in Figure 9 and an OASPL 16 dB higher.

The waveform recorded by microphone #6 shows that a strong shock wave strikes the fuselage in the propeller plane. The OASPL is 157 dB, a 22 dB increase compared to the previous case for a 19% increase in the helical tip Mach number. The very sharp waveform is responsible for an almost flat spectrum. Nine harmonics are within 10 dB from each other with the spectrum peaking at the fourth harmonic. This again points to the low blade efficiency and to the extremely high acoustic level generated by a straight thick blade at high M_h. Also, reducing the interior noise in such an airplane is a difficult task due to the wide frequency range of the noise generated.

Figure 10 shows that the maximum level of the tones is now shifted downstream compared to the previous low axial Mach number case due to the increased convection at the higher axial Mach number.

Away from the propeller plane the acoustic level still decreases rapidly and the 1 × BPF tone and its harmonics are much closer together than in Figure 9. In the propeller plane, the harmonics dominate the spectrum.

4.2. Inboard-Down Propeller Direction of Rotation

4.2.1. Angle of Attack Variation

Much work has been done recently on the effect of the angle of attack on propeller noise in order to better understand the noise generated by advanced propellers during take-off and landing (see Refs. [2] to [5]).

Figure 11 shows the directivities for the tones at 1 × BPF, 2 × BPF, and 6 × BPF, at three angles of attack. The averaged flight parameters are: $M_h = 0.88$, $M_a = 0.28$, $J = 1.04$, and $C_p = 0.097$. The maximum variation in the

flight parameters between tests is less than 3%. A few data points are missing due to a malfunction of microphone #3 during two of the tests. Results obtained for the 3, 4, and 5 × BPF tones are not presented here since they usually follow the same trend as the results for the 1, 2, and 6 × BPF tones.

For each tone, increasing the angle of attack by 9.2 degrees results in an increase in the tone level by about 5 dB to 15 dB depending on microphone position and harmonic number. This result is consistent with wind tunnel data on advanced propellers and can be simply explained by looking at the blade angle of attack variation with azimuthal angle.

Figure 12 shows the approximate propeller blade angle of attack α_b as a function of propeller azimuthal angle ψ (Equation (1)) for the three angles of attack in Figure 11.

For inboard-down rotation and for a positive α_{prop}, the angle of attack of the blade approaching the fuselage increases from a minimum when the blade is in the first quadrant (between the horizontal position away from the fuselage and the top vertical position: $0 < \psi < 90$) to a maximum when the blade is in the second quadrant (between the top vertical position and the horizontal position closest to the fuselage: $90 < \psi < 180$).

The noise generated is partly a function of the loading on the blade which is in turn a function of the blade angle of attack. From Figure 12, it is clear that when the blade is close to the microphones ($90 < \psi < 270$), the loading increases with the airplane angle of attack. This, combined with the fact that the noise generated is maximum in a direction normal to the blade radius and in

the direction of blade travel, explains the increase in the level of the tones with increasing angle of attack shown in Figure 11.

Figure 13 shows the directivities for the first six harmonics and for the lowest and highest angle of attack tested ($\alpha_{prop} = -2.5$ degrees and 8.6 degrees). The $1 \times$ BPF tone dominates the OASPL at most microphone positions for the low angle of attack case. As α_{prop} increases, the main directivity lobe of the first few tones is shifted forward. A secondary peak similar to the peak in Figure 9 appears for the $1 \times$ BPF tone aft of the propeller. The changes in acoustic level with α_{prop} are largest for the higher harmonics and in the propeller plane. At the high angle of attack, a strong shock clearly appears in the vertical array (microphones #6, #7, #8, and #9) and is strongest at the bottom of the array.

More experiments were run to study the effect of the angle of attack at different advance ratios and power coefficients as shown in the test matrix in Table III. In the range of flight parameters tested, there was no significant difference from the results presented in this section.

4.2.2. Sideslip Angle Variation

The effect of the side slip angle β_p is similar to the effect of the angle of attack. Assuming a uniform inflow to the propeller and inboard-down rotation, the noise measured on the fuselage for a positive β_p is the same as the noise measured under the airplane for a positive angle of attack (β_p is positive when the airplane left side is turned towards the downwind side). In the OV–10A case, the inflow to the propeller is not uniform due to flow distortions resulting from the small clearance between the fuselage and the propeller tip, and from the large fuselage area.

The acoustic level at each microphone for five sideslip angles is plotted on Figure 14. The averaged flight parameters are: $\alpha_{prop} = 1.1$ degrees, $M_h = 0.92$, $M_a = 0.38$, $J = 1.43$, and $C_p = 0.097$. The maximum variation in the flight parameters between tests is less than 1% except for the power coefficient C_p which varied by 7%.

Figure 15 shows the approximate propeller blade angle of attack α_b obtained using Equation (1), as a function of the propeller asimuthal angle ψ.

Since no inflow angle data in the propeller plane were available, β_p in Equation (4) was replaced by the sideslip angle β measured at the airplane boom. Therefore, Figure 15 should only be looked at as a rough indicator of the blade angle of attack, especially in the second and third quadrant ($90 < \psi < 270$) where the effect of the fuselage on the propeller inflow is the greatest.

As the sideslip angle increases from -10 degrees to $+10$ degrees, the level for each tone increases by 2 dB to 25 dB depending on microphone position and harmonic number.

From Figure 14, it is clear that most of the sound recorded at the microphones is generated when the blade angle of attack α_b increases with the sideslip angle β. According to the approximate blade angle of attack shown in Figure 15, this happens when the propeller blade is in the second quadrant ($90 < \psi < 180$) which is consistent with the fact that the noise generated by a propeller blade is maximum in a direction normal to the blade radius and in the direction of blade travel.

The effect of the sideslip angle variation on the position of the main directivity lobe is most significant for the lowest tones. As β is increased from -10 degrees

to +10 degrees, the main directivity lobe for the 1 × BPF tone is shifted from microphone #4 ($\theta \approx 70$ degrees) to microphone #7 ($\theta \approx 90$ degrees). Therefore, the angle between the maximum acoustic level for the 1 × BPF tone and the inflow tends to stay constant.

A dip appears in the directivity of the 1 × BPF tone at microphone #10 as the sideslip angle decreases. This dip, also present for the odd harmonics of the 1 × BPF tone, is most probably due to reflections from the wing interfering with direct sound radiation from the propeller. This dip was not as pronounced when the test was repeated due to slightly different flight conditions.

As with the angle of attack tests, a strong shock wave appears towards the bottom of the array as evidenced by the high level of the higher BPF harmonics recorded by microphones #8 and #9 at the bottom of the fuselage.

Tests done at a different power coefficient showed no significant change. Tests at a lower advance ratio exhibited a slightly reduced OASPL variation as a function of β and just a slight dip in the directivity of the 1 × BPF tone at microphone #10.

4.2.3. Power Coefficient Variation

The effect of the power coefficient C_p was investigated while the other flight parameters were held constant. Figure 16 shows the directivities of the tones for five power coefficients varying from 0.105 to 0.050. The averaged flight parameters are: $\alpha_{prop} = 3.3$ degrees, $M_h = 0.87$, $M_a = 0.28$, and $J = 1.08$. The variation in the flight parameters between tests is less than 1%.

The variation in the level of the tones with C_p is largest for the 1 × BPF tone. Little change in directivity is observed with varying power coefficient for

the $1 \times$ BPF tone and its harmonics. In the range of parameters tested, the effect of C_p is not as important as the effect of other flight parameters such as the angle of attack or the sideslip angle.

Variations in the acoustic levels and directivities of the tones for data acquired at a higher advance ratio were similar to the results in Figure 16.

4.2.4. Helical Tip Mach Number and Advance Ratio Variation

Due to limitations in the aircraft control system and the aircraft flight envelope, it was not possible to study the effect of the helical tip Mach number M_h alone. Therefore, between points, both M_h and the advance ratio J were allowed to vary while attempts were made to keep the other flight parameters constant.

Table IV shows the averaged values of the main flight parameters for the four test points. Efforts were made to limit the variations in the angle of attack between each point by using the aircraft flaps at low speeds and shallow dives at high speeds.

The data for the first two points ($M_h = 0.88$ and $M_h = 0.93$) were acquired during level flight, resulting in very little variation in the flight parameters between the beginning and the end of the data acquisition process (less than 1%).

The data for the last two points ($M_h = 0.98$ and $M_h = 1.05$) were acquired during high speed dives centered around a pressure altitude of 3050 meters. During the dives, it was not possible to adjust the flight conditions to maintain all flight parameters constant. Figure 17 shows the magnitude of M_h, J, and C_p at the beginning and at the end of the data acquisition process for each point.

The directivities for the four conditions tested are shown in Figure 18. As the harmonic number increases, the variation in the level of the tones with M_h also increases. For a low M_h, the 1 × BPF tone is the strongest tone. For a high M_h, the OASPL is dominated by the harmonics of the 1 × BPF tone. This result is similar to the inboard- up case presented in the introduction in Section 4.1, and is due to the strong shock wave at the propeller blade at high helical tip Mach numbers. As mentioned previously, this result points out the low efficiency of a straight thick propeller blade at high helical tip Mach numbers, as well as the wide frequency range for which attenuation is required in order to effectively reduce interior noise in such an aircraft.

4.3. Inboard-Up Propeller Direction of Rotation

For the second series of acoustic tests, the test matrix shown in Table III was flown again with both engine sets interchanged so as to change the left propeller direction of rotation from inboard-down to inboard-up. The main results are presented next with an emphasis on the effect of the change in direction of rotation. The effect of the power coefficient on the acoustic level is not included since the results obtained for both propeller directions of rotation were similar.

4.3.1. Angle of Attack Variation

Figure 19 shows the directivities of the 1 × BPF tone and some of the selected harmonics at four angles of attack. The averaged flight parameters are: $M_h = 0.85$, $M_a = 0.25$, $J = 0.95$, and $C_p = 0.094$. The maximum variation in the flight parameters between tests is less than 3%.

For inboard-up propeller direction of rotation, the level of the tones increases with decreasing propeller angle of attack (α_{prop}) which is opposite to the inboard-down case. Again, this can be explained by looking at the approximate blade angle of attack variation in Figure 20.

As shown previously, most of the noise generated by a propeller comes from the approaching blade. Therefore, for inboard-up direction of rotation, most of the noise is generated when the blade goes from the bottom vertical position ($\psi = 270$) to the horizontal position closest to the fuselage ($\psi = 180$). As the blade approaches the fuselage ($270 < \psi < 180$), Figure 20 shows that the blade angle of attack decreases with increasing α_{prop} which explains the variations in acoustic level in Figure 19.

The magnitude of the variations in the level of the tones with changes in propeller angle of attack is not as large as in the case of inboard-down direction of rotation for a similar variation in α_{prop}. This is due to the larger variation of the approaching blade α_b versus α_{prop} for inboard-down rotation than for inboard-up rotation as illustrated by Figures 12 and 20. This in turn is a result of the higher inflow angle variation at the top of the propeller plane than at the bottom due to the wing upwash (see Figure 7).

Figure 21 shows the acoustic levels at microphone #5 just ahead of the propeller plane for both propeller directions of rotation and for several angles of attack. The averaged flight parameters are: $M_h = 0.87$, $M_a = 0.28$, $J = 1.05$, and $C_p = 0.095$. The maximum variation in the flight parameters is less than 5%.

Inboard-up direction of rotation results in acoustic levels on the fuselage reduced by as much as 10 dB to 15 dB at high angles of attack compared to inboard-down rotation. Acoustic levels measured inside the cabin for inboard-up rotation showed a reduction in OASPL of 2 dB to 8 dB compared to inboard-down rotation, depending on the aircraft angle of attack.

4.3.2. Sideslip Angle Variation

Figure 22 displays the directivities of the tones for five sideslip angles. The averaged flight parameters are: $\alpha_{prop} = 1.1$ degrees, $M_h = 0.89$, $M_a = 0.37$, $J = 1.41$, and $C_p = 0.093$. The maximum variation in the flight parameters between tests is less than 1%.

The approximate propeller blade angle of attack as a function of the propeller azimuthal angle ψ is shown in Figure 23. As in the inboard-down case, the sideslip angle β is measured at the airplane nose boom. Therefore, Figure 23 is only a rough indicator of the blade angle of attack since it does not include the effect of the fuselage on the propeller inflow.

As the sideslip angle increases, the level for each tone increases. This result is similar to the inboard-down case and is easily explained by looking at Figure 23. When the propeller blade approaches the microphones ($270 < \psi < 180$) the blade angle of attack and therefore the noise increases with increasing sideslip angle.

Figure 24 shows the acoustic levels at microphone #7 for both propeller directions of rotation and for several sideslip angles. The averaged flight parameters are: $M_h = 0.91$, $M_a = 0.37$, $J = 1.42$, $C_p = 0.095$, and $\alpha_{prop} = 1.1$ degrees. The maximum variation in the flight parameters is less than 4%.

Variations in acoustic level are similar for both directions of rotation. The level of the tones on the fuselage is 2 dB to 5 dB lower for inboard-up direction of rotation than for inboard-down direction of rotation due to the different loadings of the approching blade: higher above the wing for inboard-down rotation versus lower below the wing for inboard-up rotation.

4.3.3. Helical Tip Mach Number and Advance Ratio Variation

Table V shows the averaged values of the main flight parameters for the five test points. Figure 25 shows the variation in the main flight parameters for each test point due to the change in pressure altitude during the dives.

The directivities of the tones are shown in Figure 26. The change in acoustic level with M_h is much larger than in the case of inboard-down propeller direction of rotation as a result of the combined effect of decreasing angle of attack and increasing helical tip Mach number. Due to the large differences in angle of attack between the inboard-up and the inboard-down tests, comparisons between both tests are limited.

Again, the variation in the level of the tones is largest for the higher harmonics of the 1 × BPF tone, and in the propeller plane (up to 28 dB variation for microphone #9). A slight shift in directivity in the downstream direction is observed due to increased convection at the higher axial Mach numbers.

5. Conclusions

In-flight measurements of propeller noise on the fuselage of an OV-10A Bronco airplane were obtained using a horizontal and a vertical microphone array. A wide range of flight conditions were tested including changes in angle of attack,

sideslip angle, power coefficient, helical tip Mach number and advance ratio, and propeller direction of rotation.

The main results can be summarized as follows:

1. A strong shock wave is generated by the OV-10A propeller blade even at a relatively low helical tip Mach number of 0.86. This shock wave results in high harmonic levels in the spectrum for a wide frequency range, making it more difficult to effectively control the interior noise of such an aircraft. At high helical tip Mach numbers ($M_a > 1$), the shock wave is very strong and the harmonics of the BPF tone dominate the sound pressure level on the fuselage.

2. The level of the tones at each microphone increases with increasing angle of attack for inboard-down direction of rotation and decreases for inboard-up rotation. Looking at the blade angle of attack versus azimuthal position, this opposite effect demonstrates that most of the noise generated is maximum in a direction normal to the blade radius and in the direction of blade travel. The variation in acoustic level of the BPF and its harmonics with propeller angle of attack is not as large for inboard-up direction of rotation as for inboard-down rotation. This is due to the wing upwash which causes a higher angle of attack variation between the inflow and the propeller plane at the top of the propeller plane than at the bottom.

3. The level of the tones at each microphone increases with increasing sideslip angle for both inboard-down and inboard-up directions of rotation. This is due to the increase in the blade angle of attack of the approaching blade as the sideslip angle increases for both directions of rotation.

4. An increase in the power coefficient results in an increase in the level of the BPF and its harmonics. In the range of flight parameters tested, the effect of the power coefficient is much smaller than the effect of other flight parameters such as the angle of attack or the sideslip angle.

5. The variation in acoustic level of the BPF and its harmonics as a result of changes in helical tip Mach number and advance ratio is very large. Increasing M_h and J strengthens the shock on the propeller blade thus increasing the harmonic level of the noise generated.

   In the case of inboard-up propeller direction of rotation, the combined effect of the increase in M_h and J, and the decrease in propeller angle of attack results in large differences in the level of the tones. For a 20% change in M_h and a 6 degree change in α_{prop}, a variation of as much as 28 dB was recorded in the propeller plane for the 6 × BPF tone.

References

[1.] Whitlow, J. B., and Sievers, G. K., "Fuel Savings Potential of the NASA Advanced Turboprop Program," NASA TM-83736, 1984.

[2.] Woodward, R. P., "Noise of a Model High-Speed Counterrotation Propeller at Simulated Takeoff/Approach Conditions (F7/A7)," AIAA Paper 87-2657, Oct. 1987, NASA TM-100206.

[3.] Woodward, R. P., and Gordon, E. P., "Noise of a Model Counterrotation Propeller with Reduced Aft Rotor Diameter at Simulated Takeoff/Approach Conditions (F7/A3)," AIAA Paper 88-0263, Jan. 1988, NASA TM- 100254.

[4.] Woodward, R. P., "Measured Noise of a Scale Model High- Speed Propeller at Simulated Takeoff/Approach Conditions," AIAA Paper 87-0526, Jan. 1987, NASA TM-88920.

[5.] Dittmar, J. H., "Cruise Noise of Counterrotation Propeller at Angle of Attack in Wind Tunnel," NASA TM- 88869.

[6.] Metzger, F. B., "Strategies for Reducing Propeller Aircraft Cabin Noise," Automotive Engineering, Vol. 2, No. 1, Oct. 1981.

Mic. #	x	y	z	r	θ	ϕ
	(meters)			(meters)	(degrees)	
1	2.05	-1.73	0.00	2.68	-40.3	90.0
2	1.44	-1.70	-0.00	2.22	-49.7	90.1
3	1.04	-1.73	-0.00	2.02	-58.9	90.1
4	0.60	-1.75	-0.05	1.85	-71.0	91.6
5	0.25	-1.75	-0.01	1.76	-81.9	90.2
6	-0.03	-1.72	0.33	1.75	-91.1	79.3
7	-0.05	-1.74	-0.02	1.74	-91.7	90.5
8	-0.07	-1.74	-0.33	1.77	-92.5	100.6
9	-0.03	-1.75	-0.66	1.87	-91.0	110.7
10	-0.27	-1.74	-0.00	1.76	-98.9	90.1
11	-0.67	-1.74	-0.12	1.87	-111.1	93.5
12	-1.05	-1.74	-0.01	2.03	-121.0	90.4

Table I. Microphone Positions with Respect to the Propeller Axis in Cartesian and Spherical Coordinates.

Station #	z (meters)
1	0.76
2	0.51
3	0.26
4	0.00
5	−0.26
6	−0.51
7	−0.76

Table II. Positions of Tuft Stations with Respect to the z Coordinate.

Angle of Attack Variation

J		1.08	1.08	1.08	1.42	1.42	0.96	0.96	0.96	0.96
α_{boom}		-4	1	5	-1.5	4.5	-7	-1.9	1	5
Cp	0.094	✓	✓	✓	✓	✓	✓	✓	✓	✓
	0.064	✓	✓	✓	✓	✓				

Sideslip Angle Variation

J		1.08	1.08	1.08	1.08	1.08	1.42	1.42	1.42	1.42	1.42
α_{boom}		1	1	1	1	1	-1.5	-1.5	-1.5	-1.5	-1.5
β		-10	-5	0	5	10	-10	-5	0	5	10
Cp	0.094	✓	✓	✓	✓	✓	✓	✓	✓	✓	✓
	0.064	✓	✓	✓	✓	✓	✓	✓	✓	✓	✓

Advance Ratio and Helical Tip Mach Number Variation

M_h		0.85	0.90	0.95	1.00	1.05
J		0.96	1.42	1.74	2.08	2.39
α_{boom}		3.0	-1	-3	-3.5	-4.0
Cp	0.1	✓	✓	✓	✓	✓

Power Coefficient Variation

Cp		0.10	0.09	0.08	0.06	0.05
J, α_{boom}	1.1, 1	✓	✓	✓	✓	✓
	1.5, -2	✓	✓	✓	✓	

Table III. Test matrix.

Test Point #	M_h	J	C_p	α_{prop} (degrees)
1	0.86	0.95	0.095	5.4
2	0.90	1.41	0.099	1.5
3	0.93	1.72	0.098	0.0
4	0.97	2.03	0.096	0.4
5	1.02	2.31	0.094	-0.8

Table V. Averaged Flight Parameters for the M_h and J Variation Tests. Inboard-Up Propeller Direction of Rotation.

Test Point #	M_h	J	C_p	α_{prop} (degrees)
1	0.88	0.95	0.096	-0.6
2	0.93	1.42	0.098	1.1
3	0.98	1.81	0.098	0.0
4	1.05	2.40	0.091	-0.8

Table IV. Averaged Flight Parameters for the M_h and J Variation Tests. Inboard-Down Propeller Direction of Rotation.

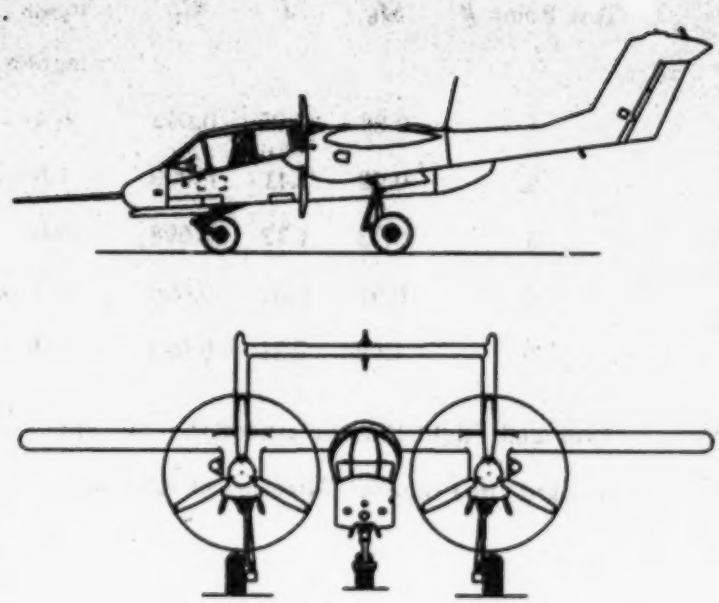

Figure 1. OV–10A Bronco Aircraft.

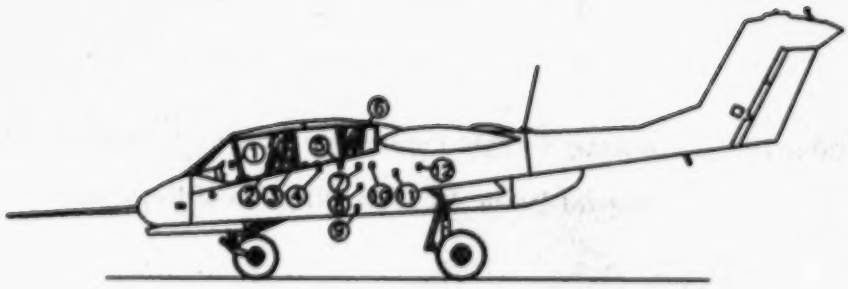

Figure 2. OV–10A Horizontal and Vertical Microphone Arrays.

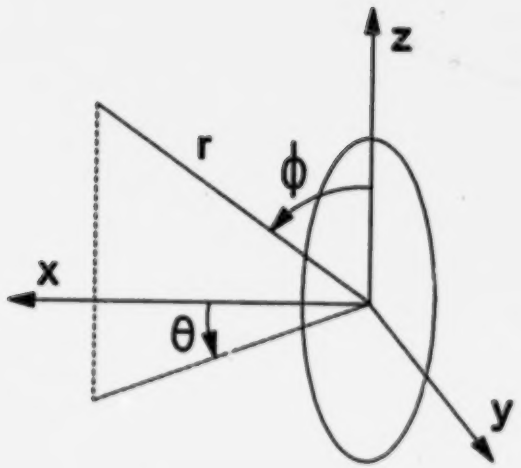

Figure 3. Coordinate Systems Used in Defining the Microphone Positions.

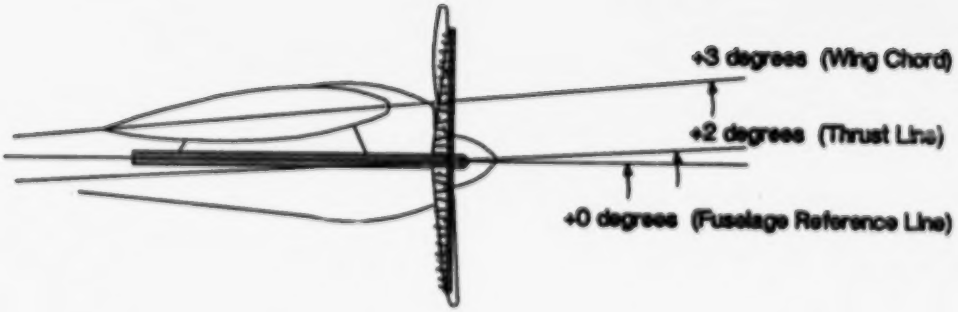

Figure 4. OV-10A Rake Used For the Inflow Angle Study.

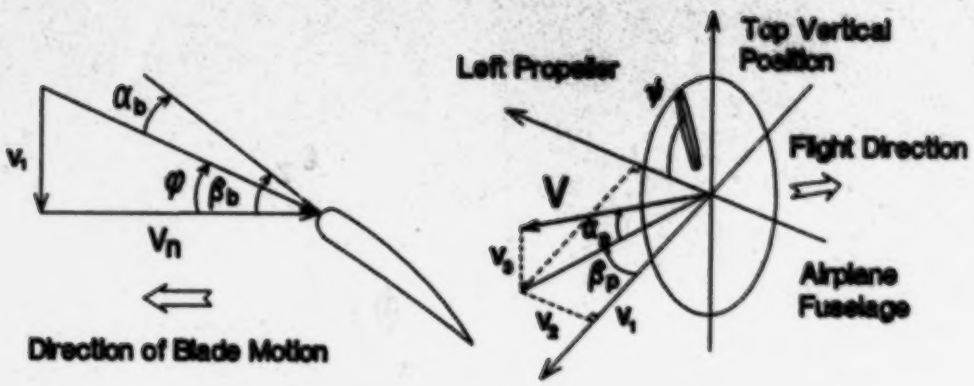

Figure 5. Propeller Blade Angle of Attack; Inflow Angles and Velocity Vectors.

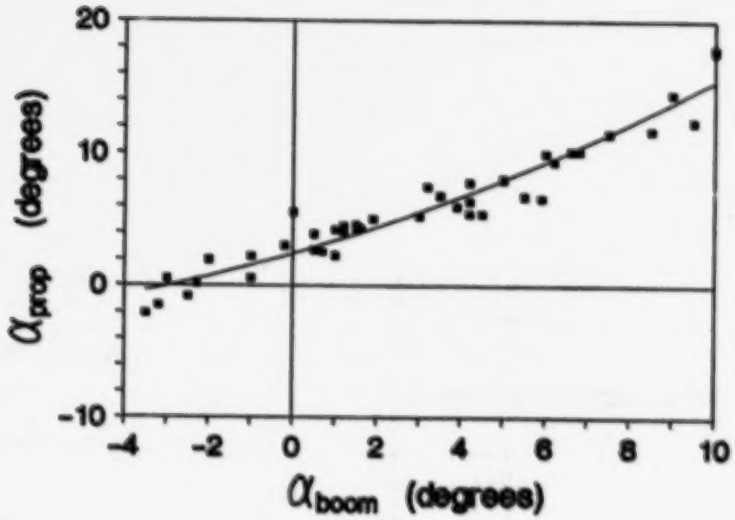

Figure 6. OV–10A Inflow Angle Study; α_{prop} versus α_{boom}.

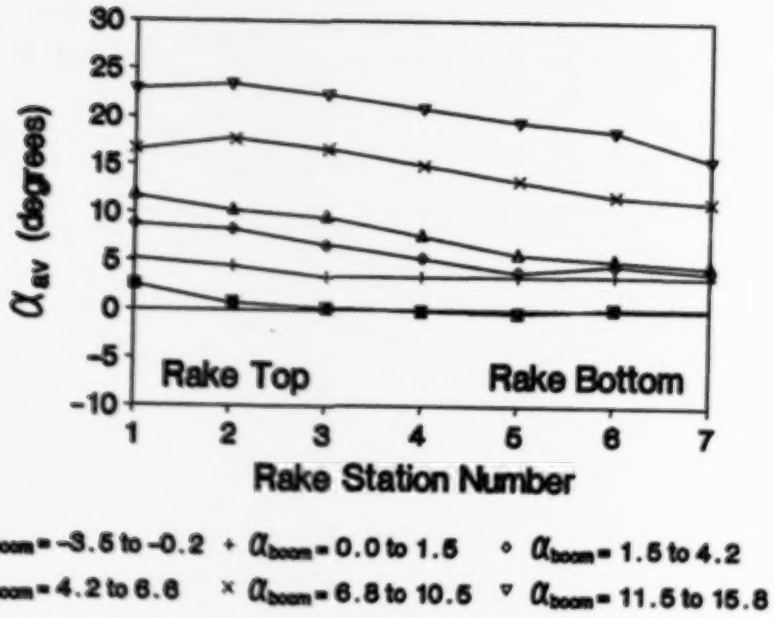

Figure 7. OV–10A Inflow Angle Study; Averaged Inflow Angles at Each Rake Station; Each Curve Represents the Average of Nine or Seven Neighboring Test Points.

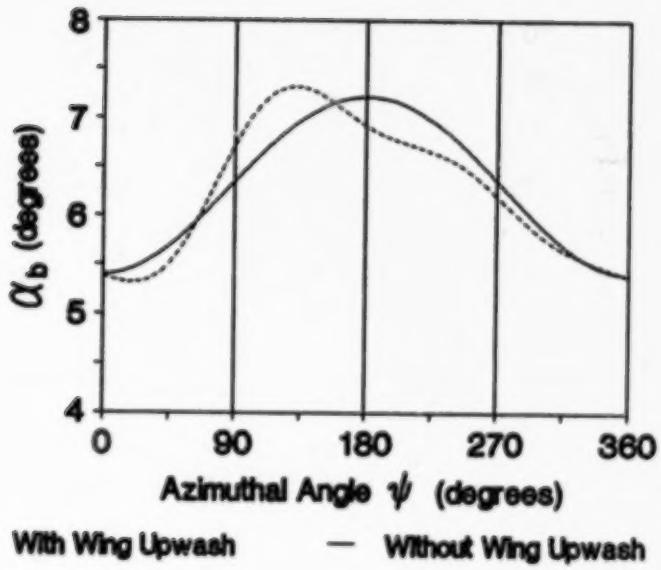

Figure 8. Left Propeller Blade Angle of Attack at the 3/4 Tip Radius Versus Azimuthal Angle For Inboard-Down Propeller Direction of Rotation With and Without Wing Upwash Effects. $\alpha_{prop} =$ 8.6 degrees, $M_h = 0.88$, $M_a = 0.28$, $J = 1.04$, and $C_p = 0.097$.

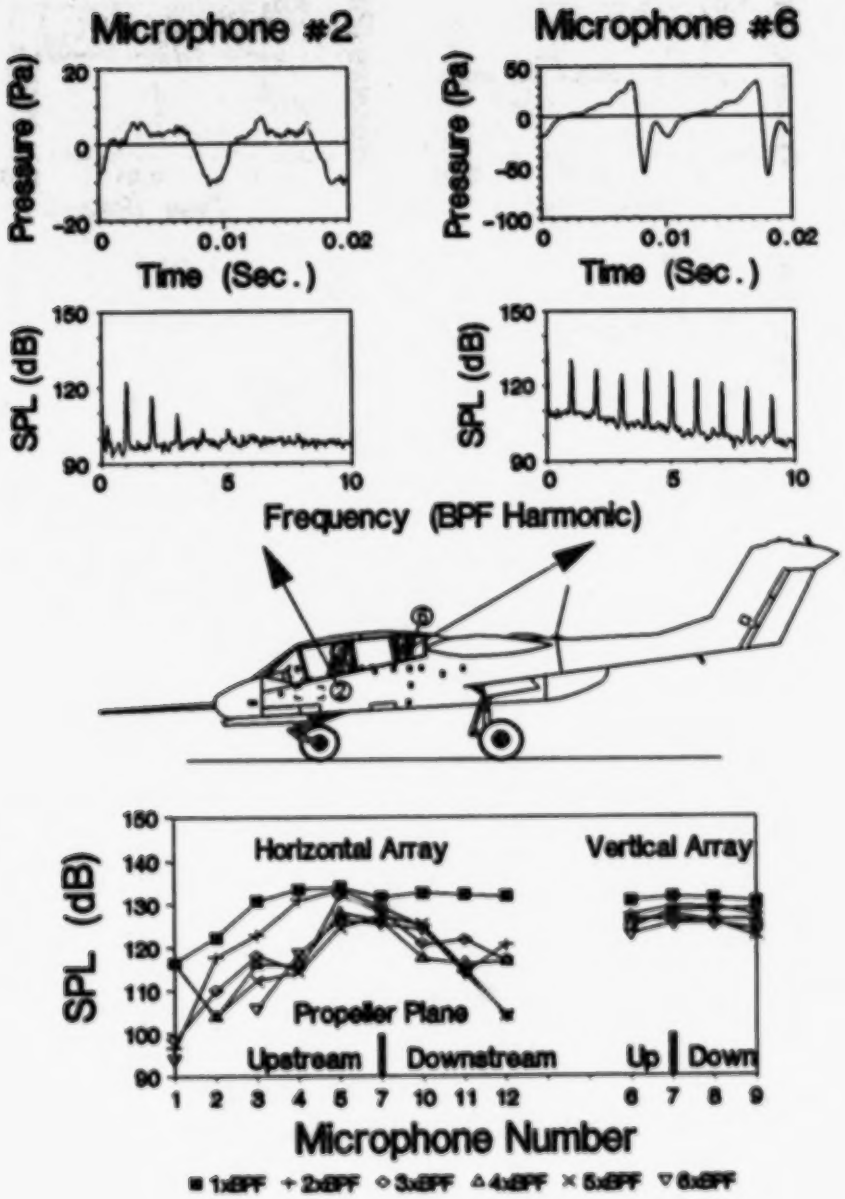

Figure 9. Acoustic Results For Moderate Helical Tip Mach Number and Inboard-Up Propeller Direction of Rotation. $\alpha_{prop} = 5.4$ degrees, $M_h = 0.86$, $M_a = 0.25$, $J = 0.95$, and $C_p = 0.09$.

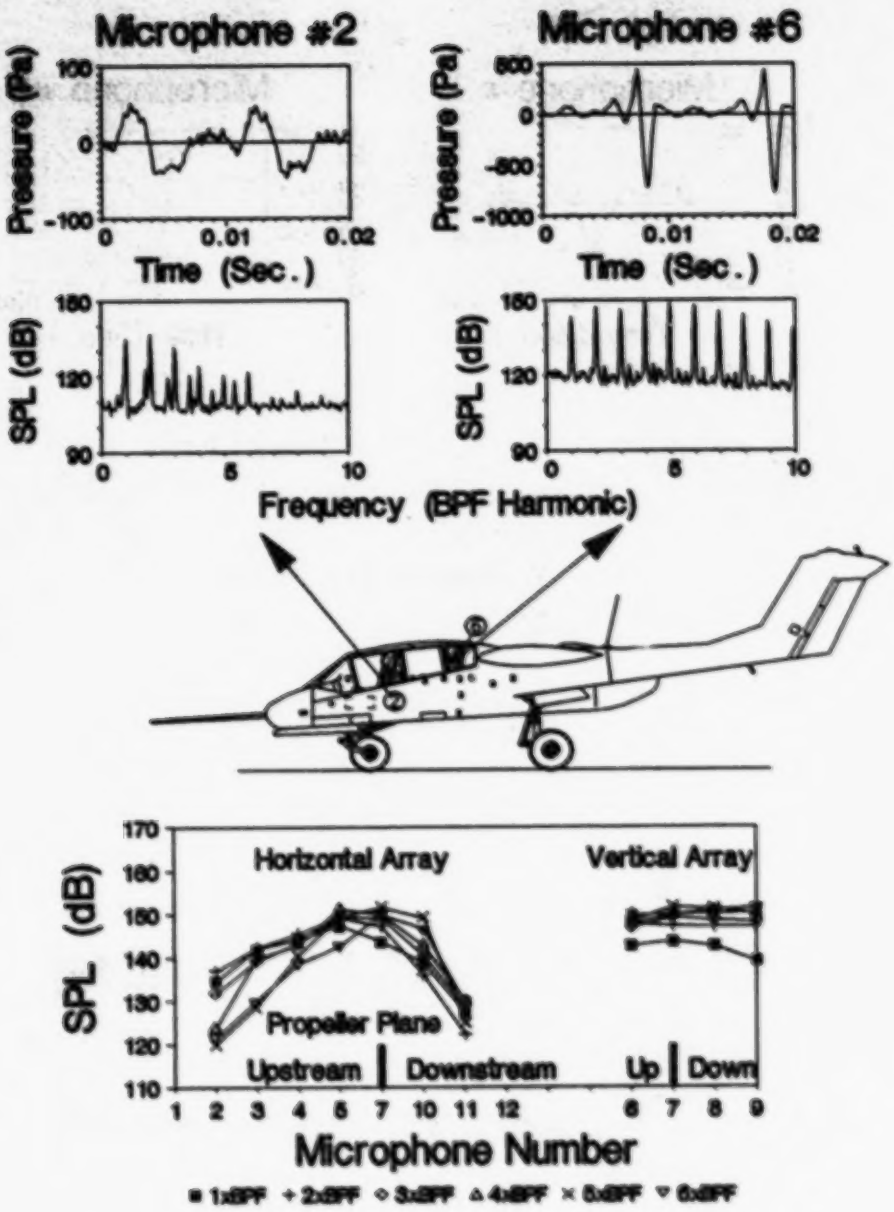

Figure 10. Acoustic Results For High Helical Tip Mach Number and Inboard-Up Propeller Direction of Rotation. $\alpha_{prop} = -0.8$ degrees, $M_h = 1.02$, $M_a = 0.60$, $J = 2.31$, and $C_p = 0.09$.

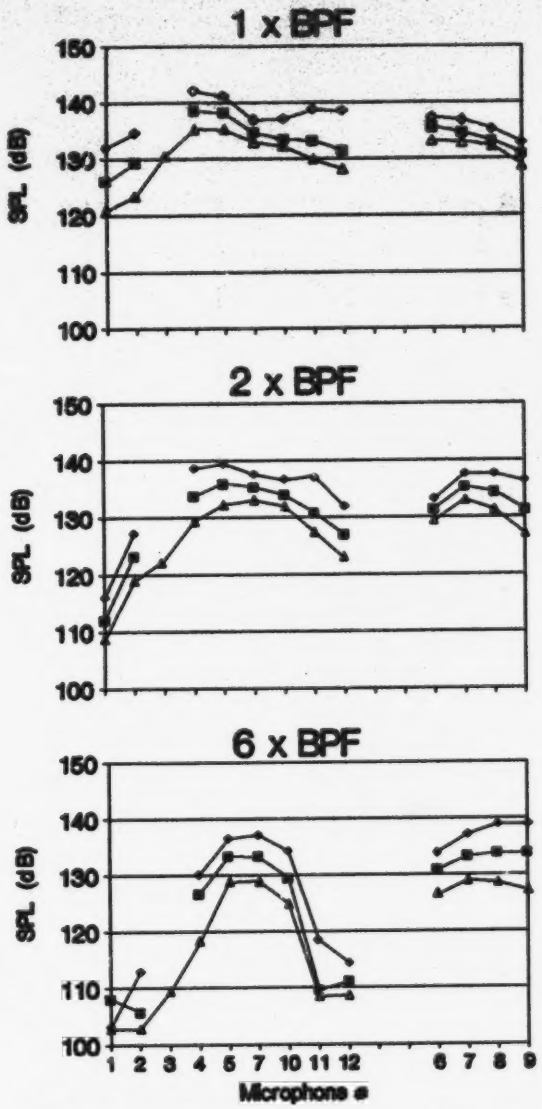

Figure 11. **Effect of Changes in Angle of Attack on the Directivities of the Tones For Inboard-Down Propeller Direction of Rotation. $M_h = 0.88$, $M_a = 0.28$, $J = 1.04$, and $C_p = 0.097$.**

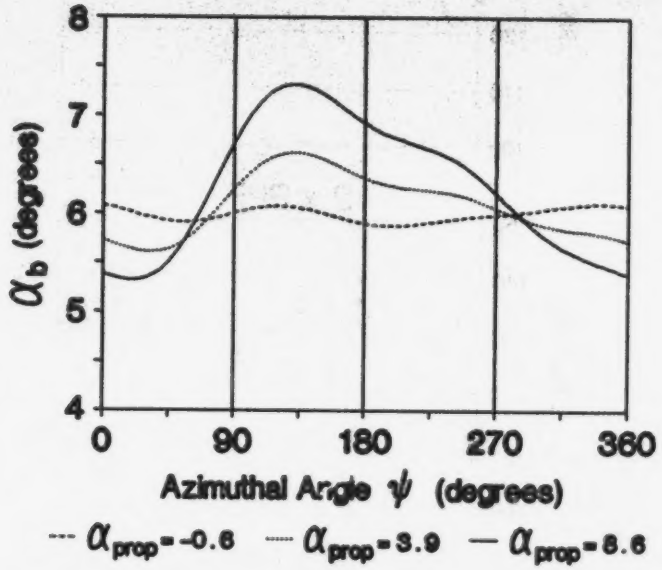

Figure 12. Propeller Blade Angle of Attack Versus Azimuthal Angle For Inboard-Down Propeller Direction of Rotation and Several Angles of Attack. $M_h = 0.88$, $M_a = 0.28$, $J = 1.04$, and $C_p = 0.097$.

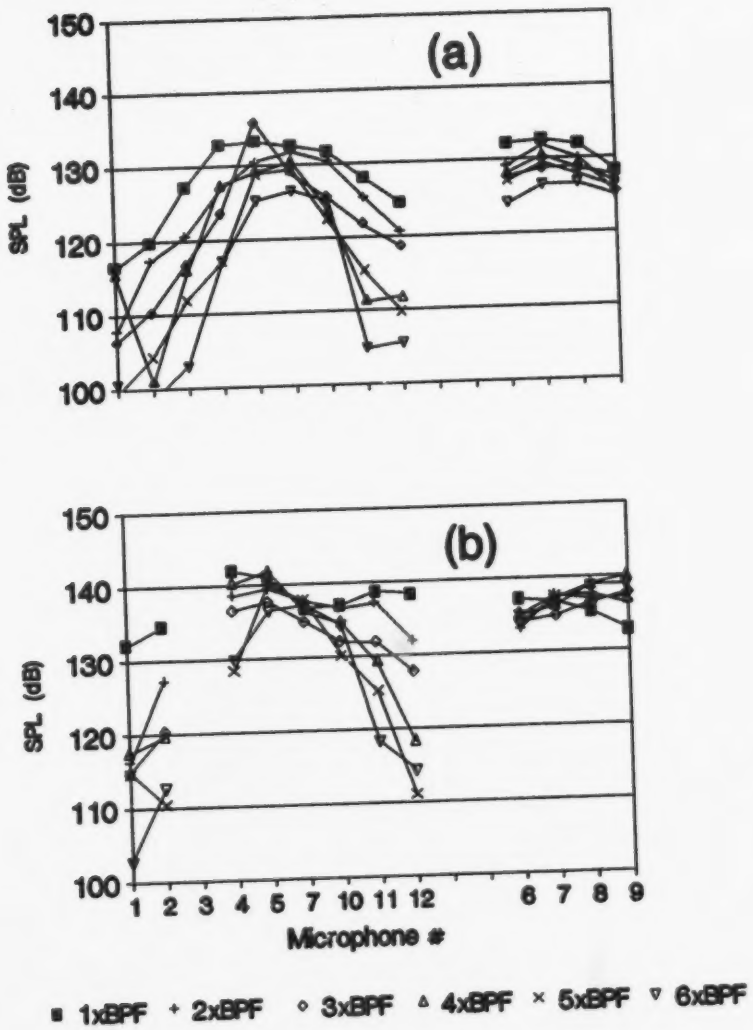

Figure 13. Directivities of the Tones For two Angles of Attack For Inboard-Down Propeller Direction of Rotation. (a): $\alpha_{prop} = -2.5$ degrees, $M_h = 0.87$, $M_a = 0.25$, $J = 0.95$, and $C_p = 0.096$. (b): $\alpha_{prop} = 8.6$ degrees, $M_h = 0.89$, $M_a = 0.29$, $J = 1.08$, and $C_p = 0.097$.

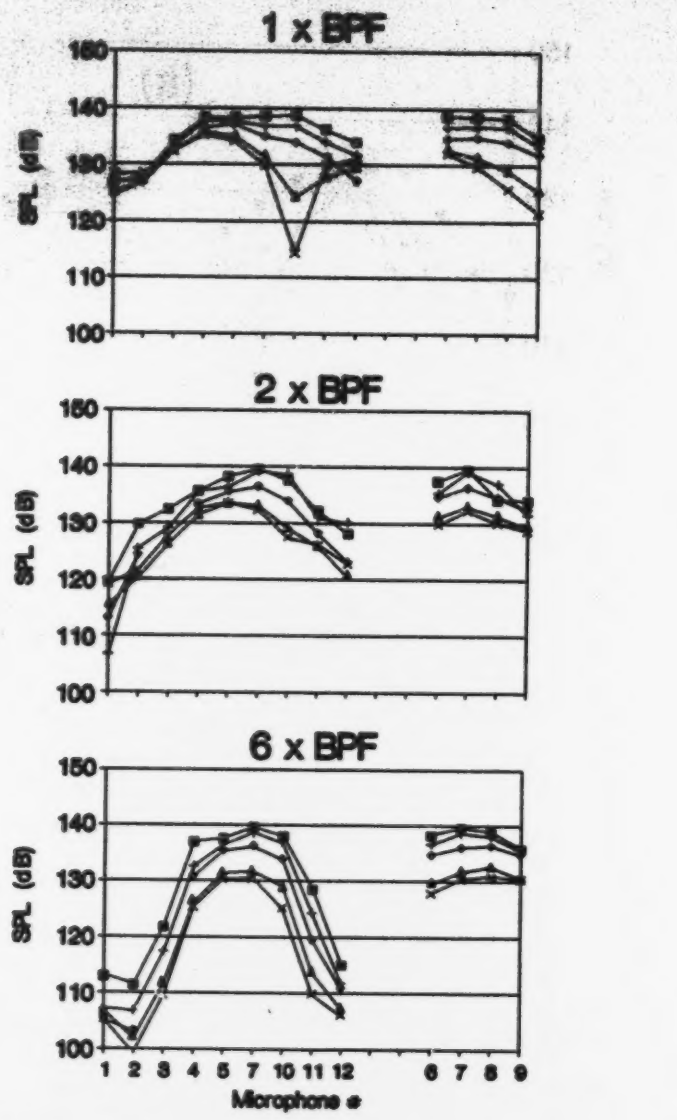

Figure 14. Effect of Changes in Sideslip Angle on the Directivities of the Tones For Inboard-Down Propeller Direction of Rotation. $\alpha_{prop} = 1.1$ degrees, $M_h = 0.92$, $M_a = 0.38$, $J = 1.43$, and $C_p = 0.097$.

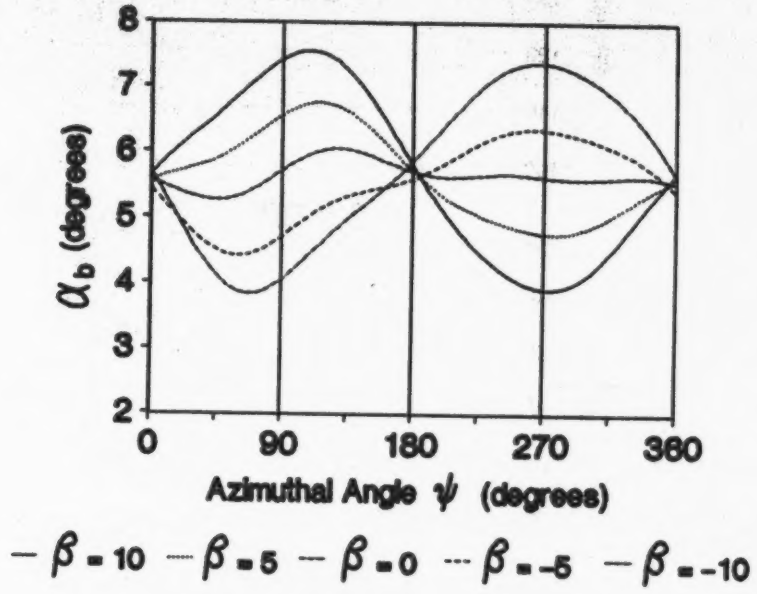

Figure 15. Propeller Blade Angle of Attack Versus Azimuthal Angle For Inboard-Down Propeller Direction of Rotation and Several Sideslip Angles. $\alpha_{prop} = 1.1$, $M_h = 0.92$, $M_a = 0.38$, $J = 1.43$, and $C_p = 0.097$.

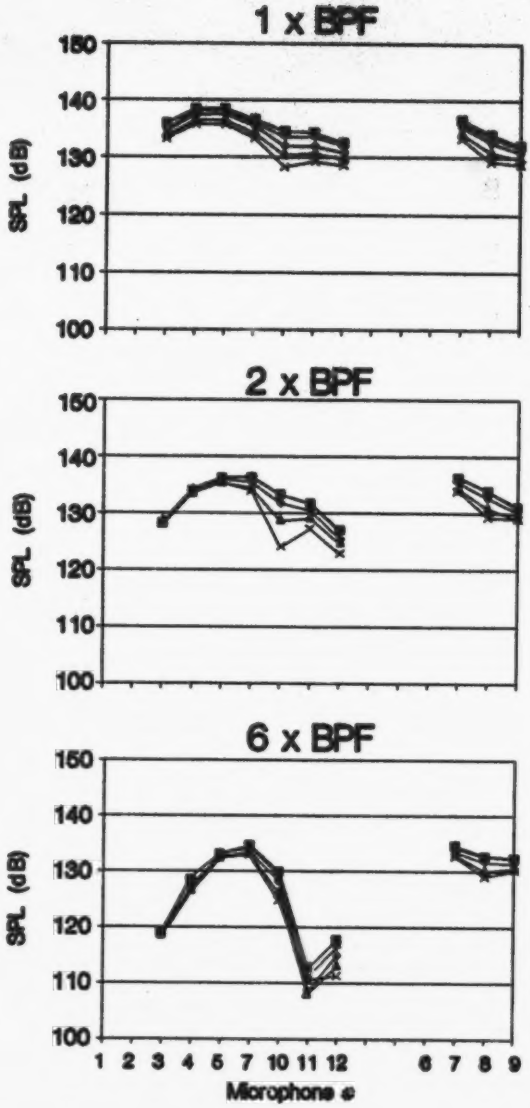

Figure 16. Effect of Changes in the Power Coefficient on the Directivities of the Tones For Inboard-Down Propeller Direction of Rotation. $\alpha_{prop} = 3.3$ degrees, $M_h = 0.87$, $M_a = 0.28$, and $J = 1.08$.

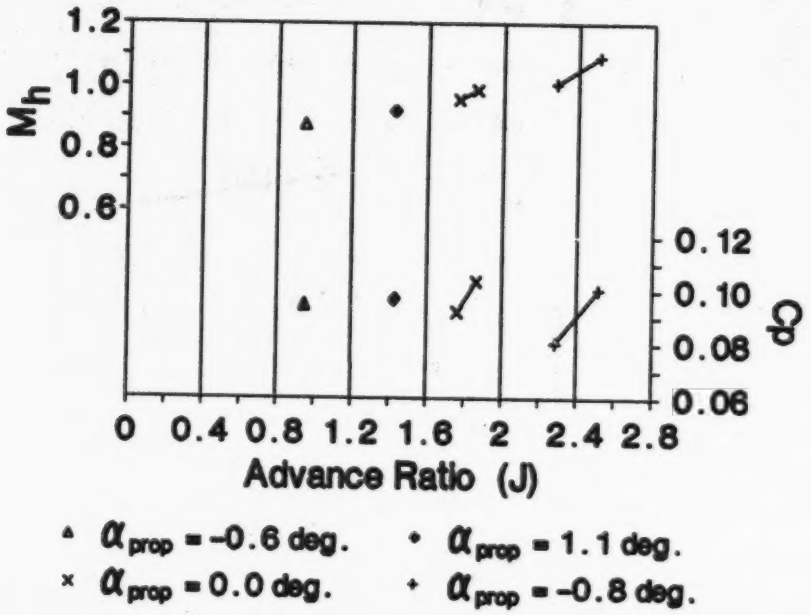

Figure 17. Changes in Flight Parameters For the M_h and J Variation Tests For Inboard-Down Propeller Direction of Rotation.

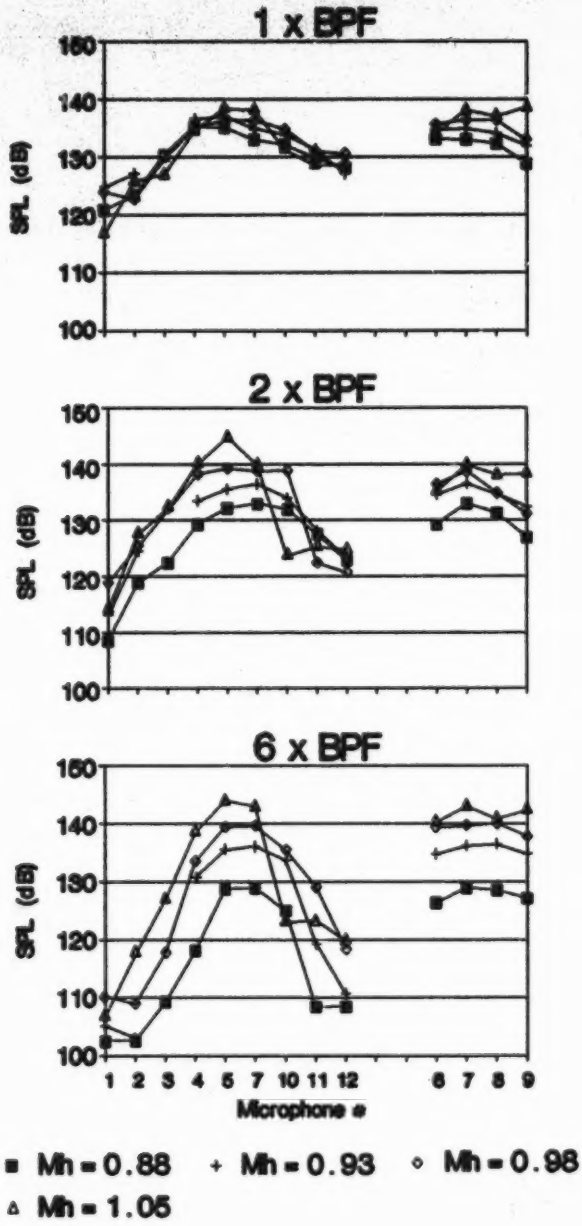

Figure 18. Effect of Changes in the Helical Tip Mach Number and in the Advance Ratio on the Directivities of the Tones For Inboard-Down Propeller Direction of Rotation.

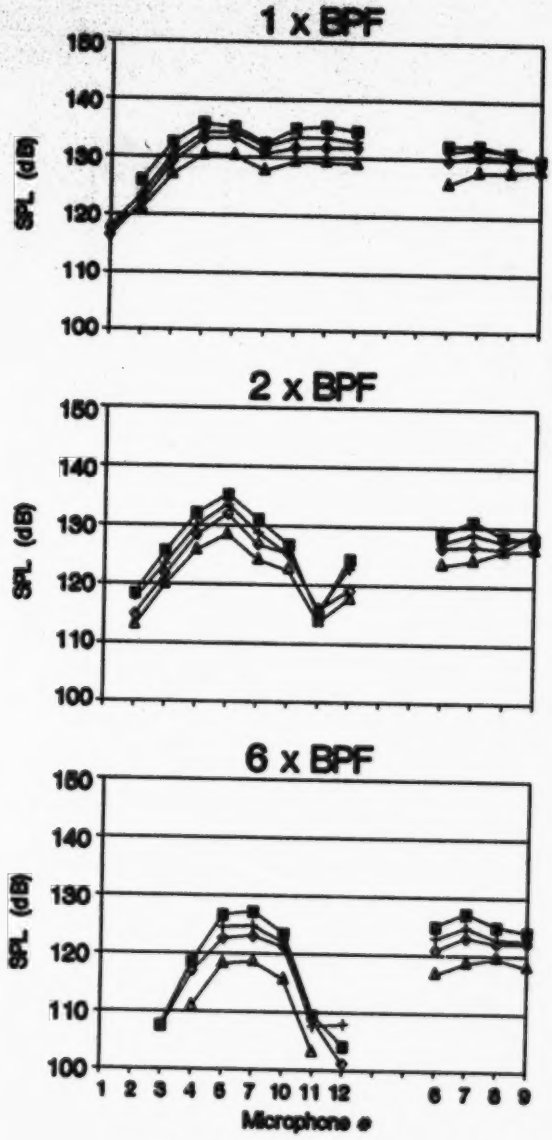

Figure 19. Effect of Changes in Angle of Attack on the Directivities of the Tones For Inboard-Up Propeller Direction of Rotation. $M_h = 0.85$, $M_a = 0.25$, $J = 0.95$, and $C_p = 0.094$.

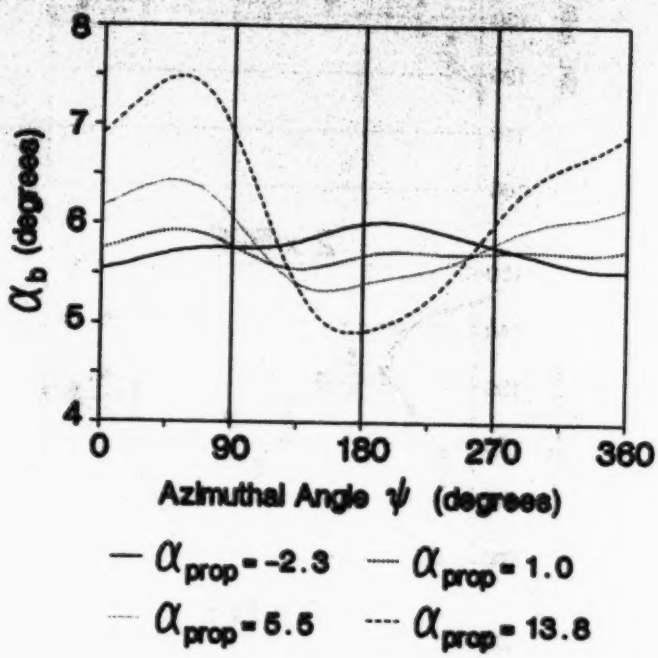

Figure 20. Propeller Blade Angle of Attack Versus Azimuthal Angle For Inboard-Up Propeller Direction of Rotation and Several Angles of Attack. $M_h = 0.85$, $M_a = 0.25$, $J = 0.95$, and $C_p = 0.094$.

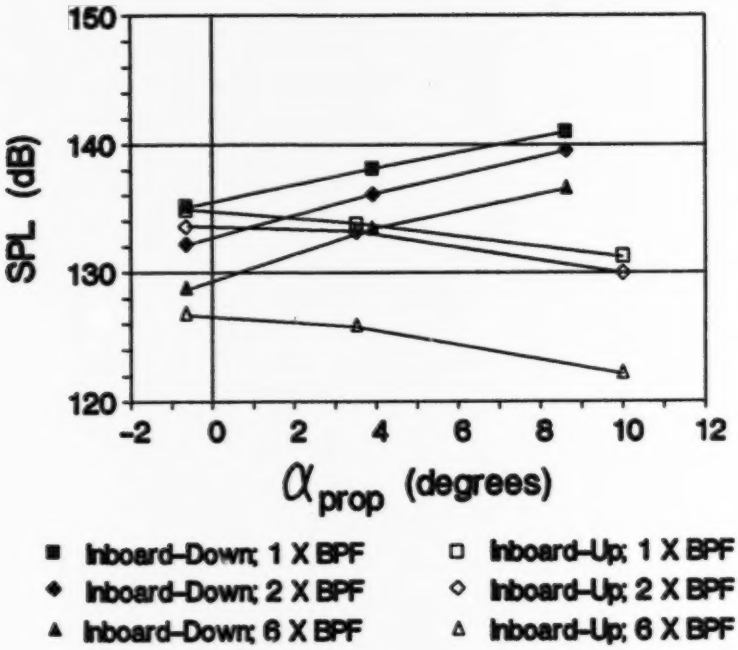

Figure 21. Tone Levels at Microphone #5 versus α_{prop} For Inboard-Down and Inboard-Up Propeller Direction of Rotation. Averaged Flight Parameters: $M_h = 0.87$, $M_a = 0.28$, $J = 1.05$, and $C_p = 0.095$.

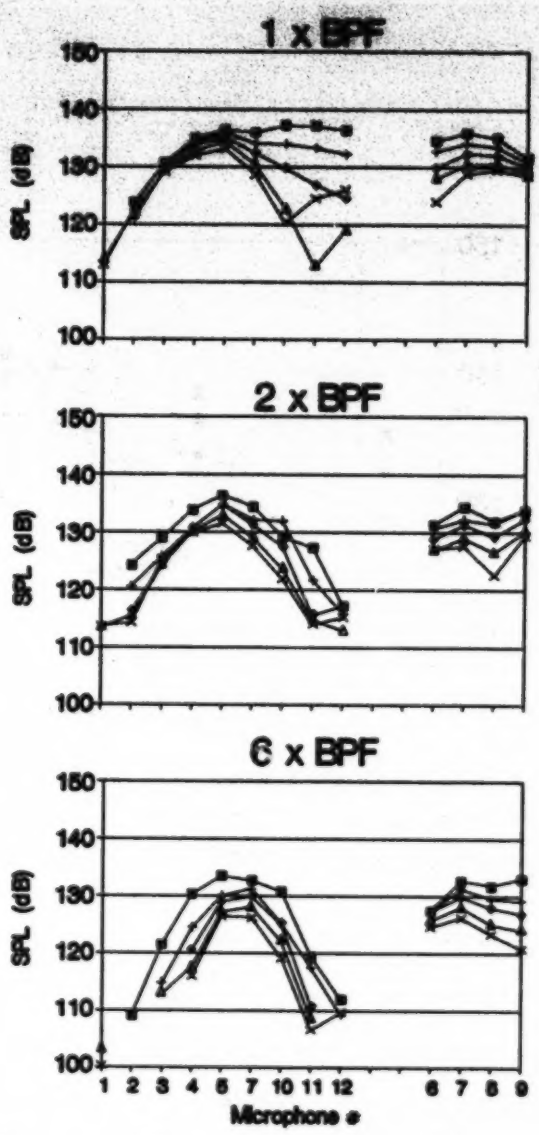

Figure 22. Effect of Changes in Sideslip Angle on the Directivities of the Tones For Inboard-Up Propeller Direction of Rotation. $\alpha_{prop} = 1.1$ degrees, $M_h = 0.89$, $M_a = 0.37$, $J = 1.41$, and $C_p = 0.093$.

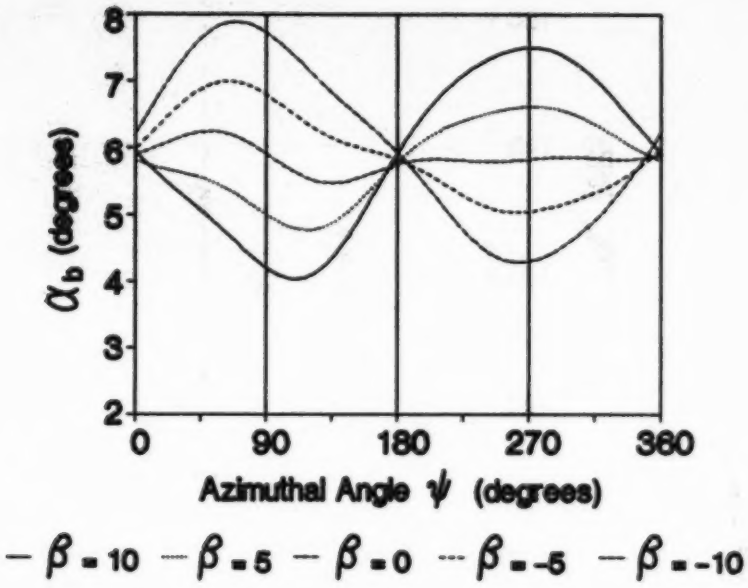

Figure 23. Propeller Blade Angle of Attack Versus Azimuthal Angle For Inboard-Up Propeller Direction of Rotation and Several Sideslip Angles. $\alpha_{prop} = 1.1$, $M_h = 0.89$, $M_a = 0.37$, $J = 1.41$, and $C_p = 0.093$.

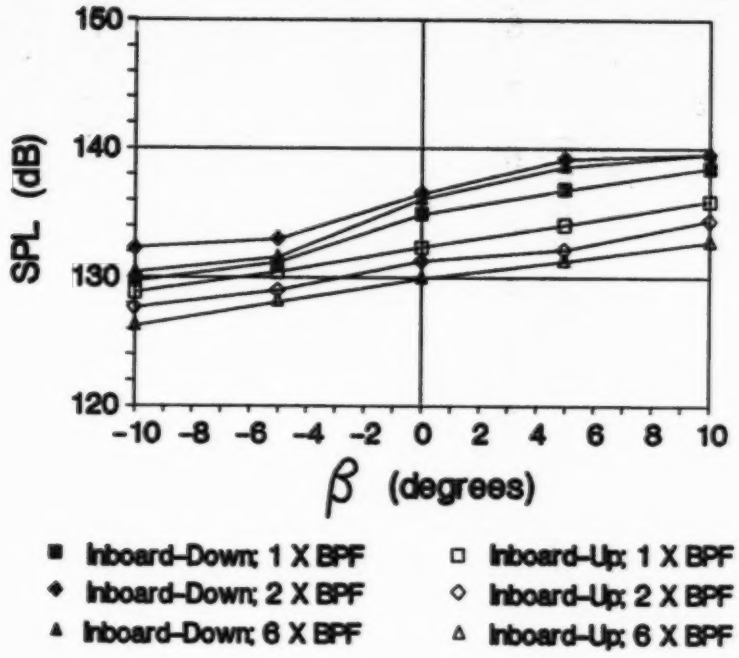

Figure 24. Tone Levels at Microphone #5 versus β For Inboard-Down and Inboard-Up Propeller Direction of Rotation. Averaged Flight Parameters: $\alpha_{prop} = 1.1$ degrees, $M_h = 0.91$, $M_a = 0.37$, $J = 1.42$, and $C_p = 0.095$.

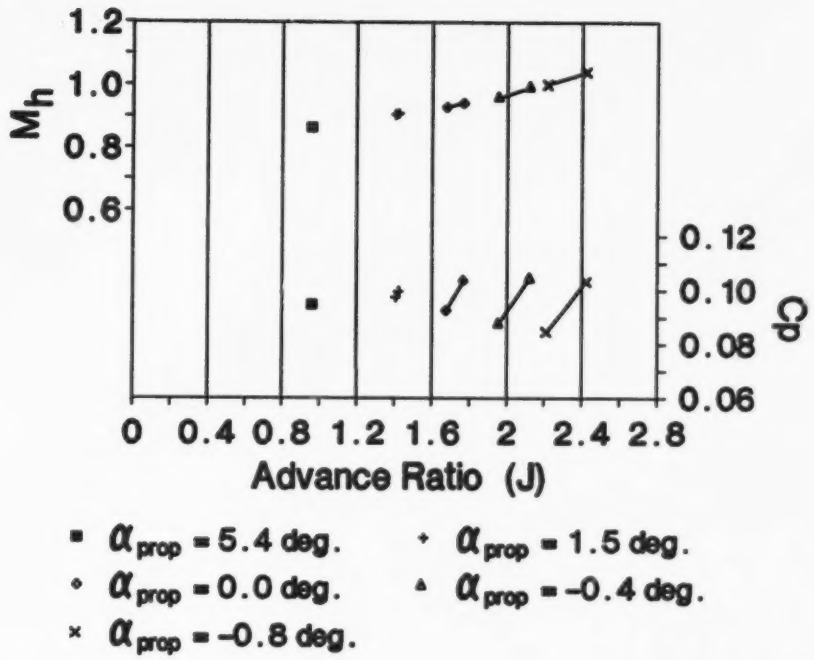

Figure 25. Changes in Flight Parameters For the M_h and J Variation Tests For Inboard-Up Propeller Direction of Rotation.

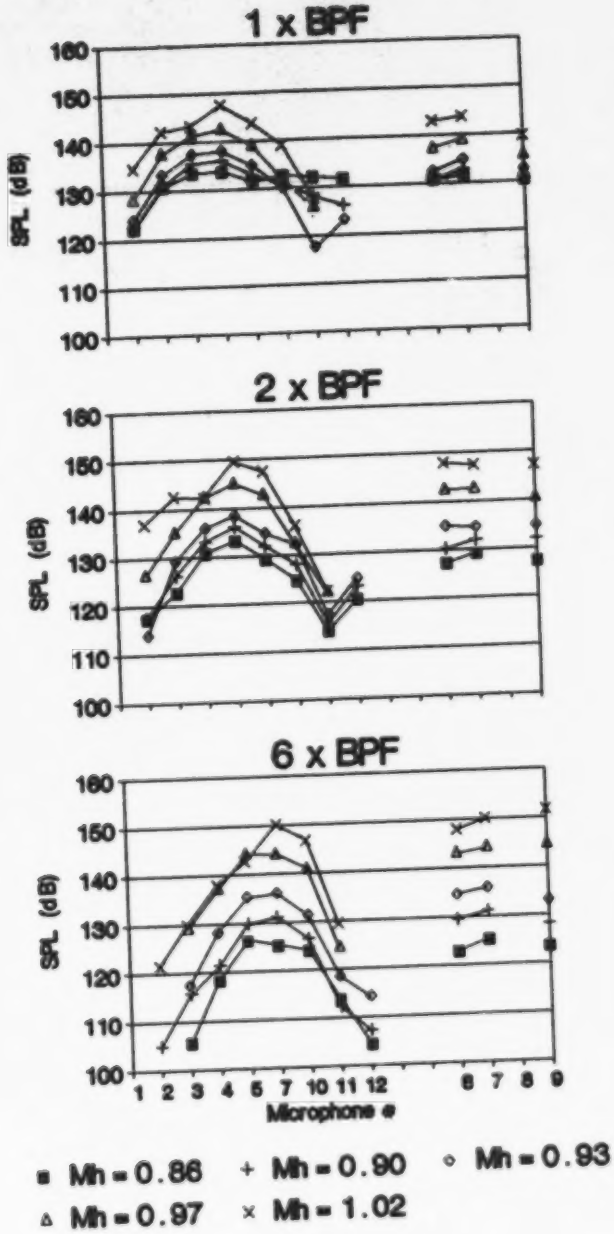

Figure 26. Effect of Changes in the Helical Tip Mach Number and in the Advance Ratio on the Directivities of the Tones For Inboard-Up Propeller Direction of Rotation.

Report Documentation Page

1. Report No.	2. Government Accession No.	3. Recipient's Catalog No.
NASA TM-102285		

4. Title and Subtitle	5. Report Date
In-Flight Measurement of Propeller Noise on the Fuselage of an Airplane	July 1989
	6. Performing Organization Code

7. Author(s)	8. Performing Organization Report No.
Frederic G. Pla, Richard Ranaudo, and Richard P. Woodward	E-4952
	10. Work Unit No. 535-03-01

9. Performing Organization Name and Address	11. Contract or Grant No.
National Aeronautics and Space Administration Lewis Research Center Cleveland, Ohio 44135-3191	
	13. Type of Report and Period Covered: Technical Memorandum

12. Sponsoring Agency Name and Address	14. Sponsoring Agency Code
National Aeronautics and Space Administration Washington, D.C. 20546-0001	

15. Supplementary Notes

Frederic G. Pla, Sverdrup Technology, Inc., NASA Lewis Research Center Group, Cleveland, Ohio 44135 (work funded under NASA Contract NAS3-24105); Richard Ranaudo and Richard P. Woodward, NASA Lewis Research Center.

16. Abstract

In-flight measurements of propeller noise on the fuselage of an OV-10A airplane were obtained using a horizontal and a vertical microphone array. A wide range of flight conditions were tested including changes in angle of attack, sideslip angle, power coefficient, helical tip Mach number and advance ratio, and propeller direction of rotation. Results show a dependence of the level and directivity of the tones on the angle of attack and on the sideslip angle with the propeller direction of rotation, which is similar to results obtained in wind tunnel tests with advanced propeller designs. The level of the tones at each microphone increases with increasing angle of attack for inboard-down propeller rotation and decreases for inboard-up rotation. The level also increases with increasing sideslip angle for both propeller directions of rotation. Increasing the power coefficient results in a slight increase in the level of the tones. A strong shock wave is generated by the propeller blade even at relatively low helical tip Mach numbers resulting in high harmonic levels. As the helical tip Mach number and the advance ratio are increased, the level of the higher harmonics increases much faster than the level of the blade passage frequency.

17. Key Words (Suggested by Author(s))	18. Distribution Statement
Propeller noise	Unclassified – Unlimited Subject Category 71

19. Security Classif. (of this report)	20. Security Classif. (of this page)	21. No of pages	22. Price*
Unclassified	Unclassified	58	A04

*For sale by the National Technical Information Service, Springfield, Virginia 22161